CHAPTER 3

Synthesis of WS_2 Nanosheets Using Surfactant-Assisted Method

Contents:

Chapter 3: Synthesis of WS_2 Nanosheets Using Surfactant-Assisted Exfoliation Method

3.1. Introduction:

The 2H-WS_2 nanosheet needs to be synthesized for the fabrication of electronic devices [1]. In this respect, different techniques have been reported for the preparation of 2D-TMD materials with good control over its morphology (nanosphere, nanosheet, nanorods, flowerlike nanostructures, etc.) and electronic band structures by varying the thickness of the TMD particle [2,3]. Top-down approaches include mostly applied methods such as chemical or liquid exfoliation [4], mechanical exfoliation [5], and electron or laser irradiation-based synthesis, while bottom-up approaches like CVD [6], MBE, ALD, and hydrothermal [7] processes are commonly used to grow 2D TMD nanomaterials.

In general, top-down synthesis methods are anticipated to be simple, cost-effective, and scalable, making them ideal for low-cost production using less advanced equipment [8–10]. The Scotch-tape method, which exfoliates materials mechanically by peeling nanosheets from bulk material, is straightforward and doesn't require a sophisticated laboratory setup. This technique produces low yields of high-quality crystalline flakes, with the exfoliated flakes having a non-uniform number of layers. However, it is a slow process with limited scalability, and the resulting sheets often have non-uniform thickness [11].

Although the CVD method offers better scalability, it faces challenges in producing highly crystalline materials. Moreover, the high temperatures (~500 ºC or more) required for deposition limit its use on flexible substrates [12,13]. Epitaxial growth on silicon-based substrates can produce continuous thin films with good crystalline quality, allowing control over the thickness, size, shape, and number of layers. However, transferring these nanosheets to the desired substrate remains difficult [14]. The hydrothermal method, which involves the use of simple equipment, grows nanosheets at moderate temperatures (200-300 °C) and allows for the synthesis of large quantities. Nevertheless, achieving high-quality 2D materials with uniform thickness and size is still a challenge [13,15]. The method is widely used because of its simplicity, but the lack of precise control over material dimensions often results in variability in the structural and functional properties, making it less suitable for applications that require consistency and precision.

Therefore, there is a need to develop an environmentally friendly method for the controlled growth of atomic-scale, few-layered WS_2 nanosheets at low temperatures, enabling their application in a wide range of electronic devices. Developing a simple, efficient, low-cost, and eco-friendly LPE technique in aqueous solution remains a priority to enhance the potential applications of WS_2 in semiconductor applications. This approach eliminates the need for harmful chemicals or toxic gases [9,16–20]. In the LPE process, selecting a suitable solvent and surfactant enables the production of highly concentrated and stable suspensions. So far, Cyclohexylpyrrolidone (CHP), NMP, DMF, Polyethylene Glycol (PEG), Hexamethylenetetramine (HMT) has proven to be the most effective solvents for achieving high-yield exfoliation of TMD materials [8,21]. These solvents are particularly advantageous due to their compatibility with the surface energy of 2D materials, which facilitates effective exfoliation. Additionally, their ability to form stable dispersions in organic solvents ensures the long-term stability and high yield of exfoliated nanosheets. [2,11,12,14]. The widespread application of these exfoliating agents is still limited due to their toxic and flammable nature, environmental hazardous, etc. In addition, processing the obtained nanosheets into films and composites seems challenging due to their high boiling points [20,22,23]. The process is also associated with high solvent cost and prolonged sonication times, which weakens their use for cost-effective research applications. On the other hand, DI water, ACE, and EtOH can be employed to produce WS_2 nanosheets with a thickness of ~4-10 nm followed by a long-time sonication process. [24, 25]. However, these low-boiling-point solvents often result in low efficiency and are less effective for exfoliating nanosheets from bulk TMDs [24–26]. Organic solvents such as Sodium Cholate (SC), Cetyltrimethylammonium Bromide (CTAB), etc. offer advantages like compatible surface energy with 2D material, stable dispersibility, high yield as well as the process is non-hazardous, eco-friendly in nature [11,12,27,28]. Table. 3.1 summarizes the representative works on liquid phase exfoliation of WS_2 materials using various exfoliating agents.

Surfactant-assisted LPE process is one of the most common and versatile techniques for exfoliating WS_2 and other TMD materials. Surfactants are generally categorized based on their ionicity, which is classified into three distinct types: anionic, cationic and non-ionic [28]. Sodium Dodecyl Benzene Sulfonate (SDBS), an anionic surfactant helps to exfoliate the WS_2 material in an aqueous solution and the ultrasonic

vibration is used to separate the nanosheets from bulk WS_2 powder [27,29–31]. SDBS recognized for its affordability, environmental compatibility, and exceptional performance as a surfactant is a commercial detergent, that presents a viable approach to achieving this goal. This study emphasizes a simple and effective LPE technique for producing WS_2 nanosheets, utilizing SDBS as a stabilizing agent to achieve an environmentally sustainable synthesis process. Spectroscopic analyses of Raman, UV-Vis, PL, XRD, AFM, FESEM, and HRTEM were conducted to optimize surface morphology, crystal size, crystalline nature, layer count, and flake thickness.

Table 3.1: Summary of representative works on LPE of WS_2 using different exfoliating agents

Exfoliating Agent	Lateral Size	Thickness	Sonication Time	Number of Layers	Ref. No.
DMF	Few hundred nanometer	6 nm	12 hr	Few-layer	[2]
ACE	≥200 nm	6nm	10 hr	Few-layer	[24]
MeOH	≥150 nm	5nm	10 hr	Few-layer	
EtOH	≥120 nm	5nm	10 hr	Few-layer	
IPA	≥150 nm	4nm	10 hr	Few-layer	
IPA	~1.2 µm	0.86-3.62 nm	1- 13 hr	1-2	[25]
DI Water	<200 nm	2-3 nm	8 hr	Few-layer	[26]
SC	50-400 nm	30-40 nm	2 hr	>10	[28]
NMP	Few hundred nanometer	3 nm	3 hr	Few-layer	[32]
DMF	2-3 µm	Few nanometer	5 hr	1-5	[33]
CHP	~40 nm-1µm	-	2.5 hr	1-5	[34]
PEG	~200 nm	~27 nm	30 min	-	[35]
NH_3	200 nm	2-8 nm	3 hr 45 min	2-6	[36]
$(NH_4)_2CO_3$	400 nm	3 nm	2 hr	2-5	[37]
SC	25–200 nm	1.6-9 nm	6 hr	2-5	[38]
CTAB	90 nm	-	8 hr	-	

3.2. Liquid Phase Exfoliation Method of WS_2 Nanosheets:

The liquid phase exfoliation process flow of WS_2 nanosheets is pictorially depicted in Fig. 3.1. In the LPE process, the bulk WS_2 powder (0.12 gm) with different concentrations of SDBS dissolved in DI water (50 ml). The prepared solution was sonicated using a horn probe sonic tip for 6 hr-10 hr (~124 W) with 60 secs ON and 5 secs OFF pulse state and to avoid excessive heating of the probe, an ice bath was used. The sonicated solution was centrifuged at 3000 rpm for 30 min, which can help to separate

the exfoliated and unexfoliated samples. Then the top of the supernatant was decanted for further use.

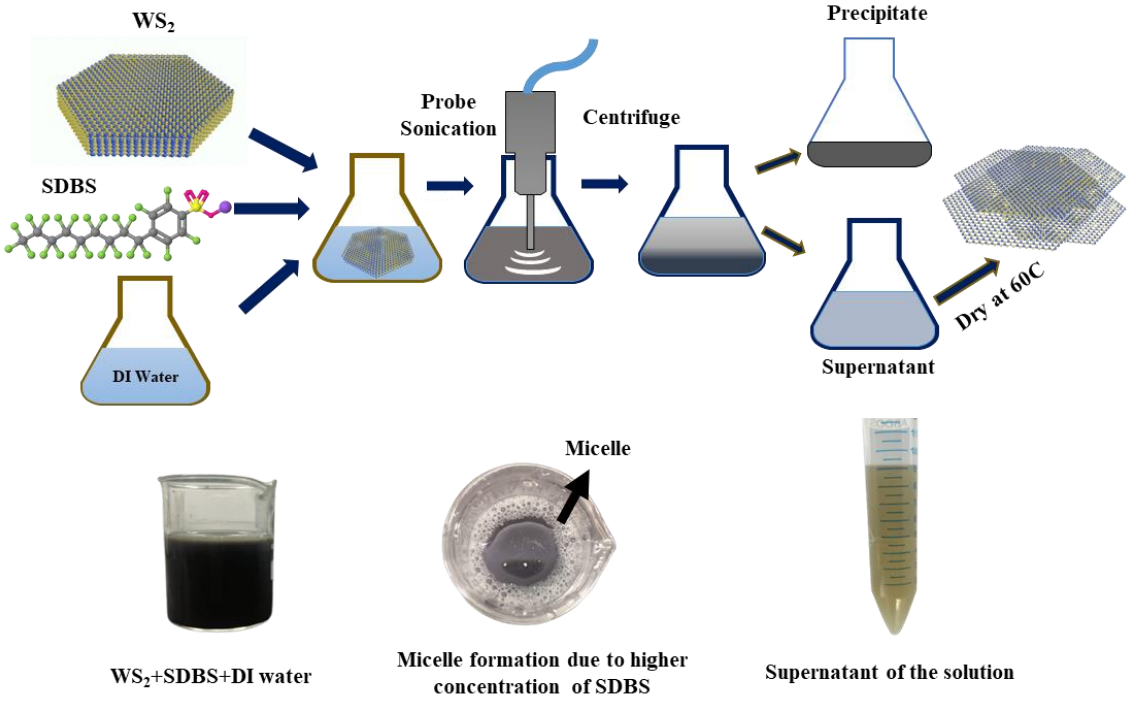

Fig. 3.1: Schematic depiction of the sequential steps of Liquid-phase exfoliation of the WS_2 nanosheet

Table 3.2: Experimental Parameters for SDBS-Assisted Exfoliation of WS_2 Nanosheets

Surfactant Type	SDBS Const. (µmol/ml)	WS_2 Concentration	Sonication Power (W)	Sonication Time (hr)	Centrifuge Speed (rpm)
SDBS is an anionic surfactant commonly used as an exfoliating agent in aqueous solutions.	2.29	0.12 gm	~124 W	6, 8 and 10 hr	3000 rpm
	4.30				
	5.16				
	6.02				
	6.88				

The collected supernatant was washed with DI water to remove the adsorbed surfactant from the exfoliated WS_2 nanosheets and dried at 60 ^oC in a hot air oven. Various spectroscopic measurements were performed to analyse their crystalline structure, material properties, nanosheet thickness, etc. The prepared samples are determined as S1 for bulk WS_2 and S2-S6 for SDBS concentrations of 2.29 µmol/ml, 4.30 µmol/ml, 5.16 µmol/ml, 6.02 µmol/ml and 6.88 µmol/ml, respectively.

3.3. Spectroscopy Measurements:

3.3.1. Raman Spectroscopy:

Raman spectroscopy is one of the primary methods to identify the chemical structure, crystalline nature, and layer numbers in 2D materials. Fig. 3.2 shows the Raman spectra excited by 514 nm and 532 nm laser at room temperature for bulk WS_2 and exfoliated WS_2 nanosheets with different concentrations of SDBS and with varying sonication time. In Raman spectroscopy, the WS_2 material is primarily identified by two vibrational frequency peaks: the out-of-plane A_{1g} mode and in-plane E^1_{2g} mode [39]. The frequency peaks of A_{1g} and E^1_{2g} are located at ~419.8 cm^{-1} and ~350.1 cm^{-1}, respectively, for bulk WS_2 and the peak difference of these two peaks is 69.7 cm^{-1} as shown in Fig 3.2(a). This agrees with the work reported by Huang et al. and Jeffery et al. [33, 40]. The frequency peak characteristics of the exfoliated samples are summarized in Table 3.3. The data in Table 3.3 indicate that after exfoliation frequency peak difference between E^1_{2g} and A_{1g} decreases from 69.7 cm^{-1} (S1) to 65.15 cm^{-1} (S4: 6 hr sonication) as shown in Fig. 3.2(b). However, when the SDBS concentration is increased beyond 6.02 µmol/ml for sample S5, which corresponds to the critical micelle point of the surfactant, the frequency peak difference between the E^1_{2g} and A_{1g} starts increasing, indicating the inefficiency of the exfoliating agent. The results indicate that the surfactant concentration plays a critical role in the exfoliation of WS_2 layers. Additionally, extending the sonication time from 6 hr to 10 hr for sample S4 results in noticeable changes in peak intensity and peak difference, as shown in Fig. 3.2(c). The reduced peak difference and increased intensity confirm the exfoliated WS_2 consists of a nanosheet in a few layers, a finding further supported by AFM analysis [36,41]. Another notable observation is the presence of the second-order longitudinal acoustic 2LA(M) mode at ~321 cm^{-1} in all exfoliated samples, though its intensity is relatively weaker in bulk WS_2. Peak stiffening was observed for all the exfoliated samples, as evidenced by the full width half maximum (FWHM) of the E^1_{2g} and A_{1g} modes in Raman spectra. The FWHM values for the E^1_{2g} and A_{1g} modes are 21.55 and 15.54 for bulk WS_2, respectively, decreasing to 17.3 and 11.1 for sample S4. However, the FWHM values increase again for samples S5 and S6. These results are consistent with the findings of Huang et al. and Zhou et al.[33, 42]. From the Raman spectroscopic analysis, indicates that the exfoliation strength of

WS_2 initially increases with rising SDBS concentration, as evidenced by the decreasing peak difference between E^1_{2g} and A_{1g}. The maximum exfoliation occurs in sample S4. Thus, further characterization is focused on sample S4 with exfoliation times of 6 hr, 8 hr, and 10 hr.

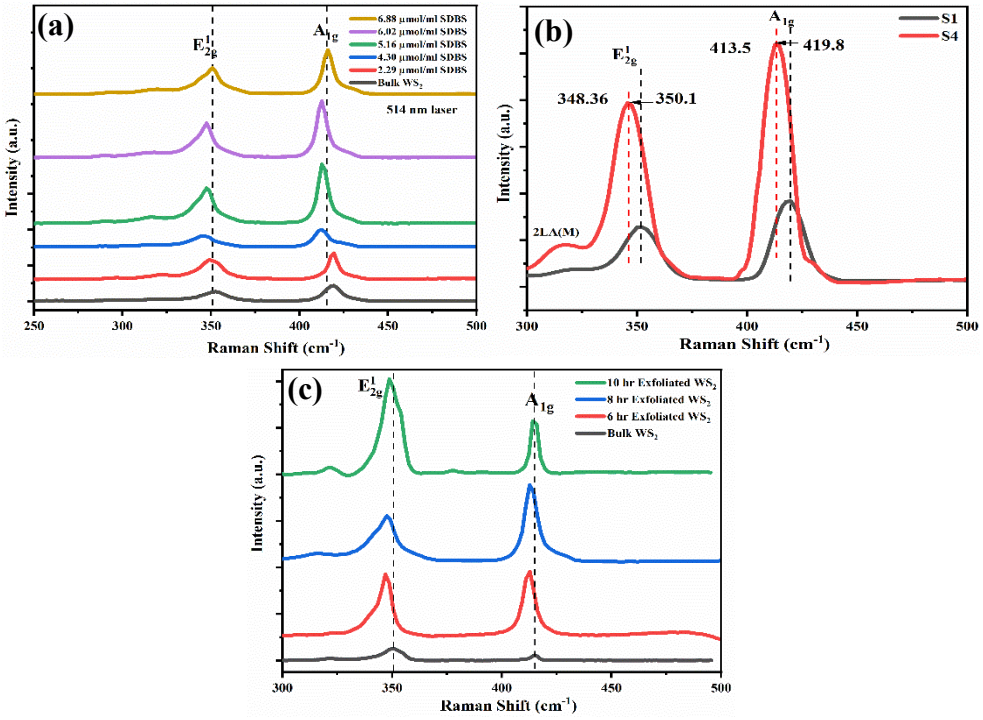

Fig. 3.2: (a) Raman spectroscopy of the exfoliated 6 hr WS_2 nanosheets was taken using a 514 nm laser for the surfactant concentration of 2.29 µmol/ml, 4.30 µmol/ml, 5.16, 6.02 and 6.88, (b) reduce the peak frequency difference (A_{1g}-E^1_{2g}) from 69.7 cm^{-1} for bulk WS_2 to 65.15 cm^{-1} for 6 hr exfoliated WS_2 and (c) the difference of Raman spectra after increasing the WS_2 exfoliation time from 6 hr to 10 hr at a surfactant concentration of 5.16 µmol/ml was measured using a 532 nm laser

Table 3.3: Characteristic of the frequency peak of bulk and exfoliated WS_2 samples

Sample ID	Const. of SDBS (µmol/ml)	2LA(M) (cm^{-1})	Peak diff. A_{1g} -E^1_{2g} (cm^{-1})	Intensity Ratio	FWHM (cm^{-1})	
					E^1_{2g}	A_{1g}
S1	Bulk WS_2	319.58	69.7	0.5659	21.5	15.5
S2	2.29	320.5	69.2	0.92	20.7	13.4
S3	4.30	323.33	67.8	0.61	18.9	12.3
S4	5.16	319.03	65.15	0.54	17.3	11.1
S5	6.02	319.27	66.1	0.54	17.6	11.4
S6	6.88	319.82	67.1	0.54	18.7	11.6

3.3.2. UV-Vis Spectroscopy:

The absorption spectra of the WS_2 nanosheets as a function of wavelength were measured using UV-Vis spectroscopy for exfoliated samples as presented in Fig 3.3. This measurement was employed as an alternative method to unambiguously determine the number of layers for collected nanosheets after dissolving in DI water [43]. The three-excitation peaks observed in the absorption spectra are obtained at ~631 nm, ~526 nm and ~463 nm which are denoted as A, B and C, respectively as depicted in Fig. 3.3(a). The excitonic transitions corresponding to peaks A and B are situated at the K-point of the Brillouin zone. In contrast, peak C, occurring at a shorter wavelength, is associated with the Γ-point. This peak is attributed to the density of states present between the valence and conduction bands [43,44]. The position of peak B corresponds to a slightly lower wavelength originating from the transitions of the split lower valance band to the conduction band. The energy difference between peaks A and B, approximately 0.4 eV is attributed to spin-orbit splitting in the valence band [24,32]. Moreover, the absorbance intensity and the red-shift of the excitonic peak qualitatively indicate a decrease in the number of layers within the nanosheet. The splitting of the valence band in multilayer nanosheets arises from the combined influence of spin-orbit coupling and interlayer interactions [43]. A red-shift in the absorbance peak was observed with an increase in exfoliation time, which means a decrease in the number of layers, as confirmed by UV-Vis as demonstrated in Fig. 3.3(b). Moreover, the absorbance spectra of 10 hr exfoliated nanosheets after being centrifuged at various speeds are shown in Fig. 3.3(c). At lower rpm, the peaks show higher intensity than at higher rpm. The bandgap of the 10 hr exfoliated nanosheet, derived from the Tauc plot, can be seen in Fig. 3.3(d). The results demonstrate the fabrication of multilayer nanosheets by LPE procedure.

The average Nanosheet Thickness (*N) is* approximately <10 nm in dispersion was determined from the wavelength of A exciton (λ_A) using the method outlined by Backes et al. for WS_2 [31]_

$$N = 6.35 \times 10^{-32}\, e^{\lambda_A/8.51} \tag{3.1}$$

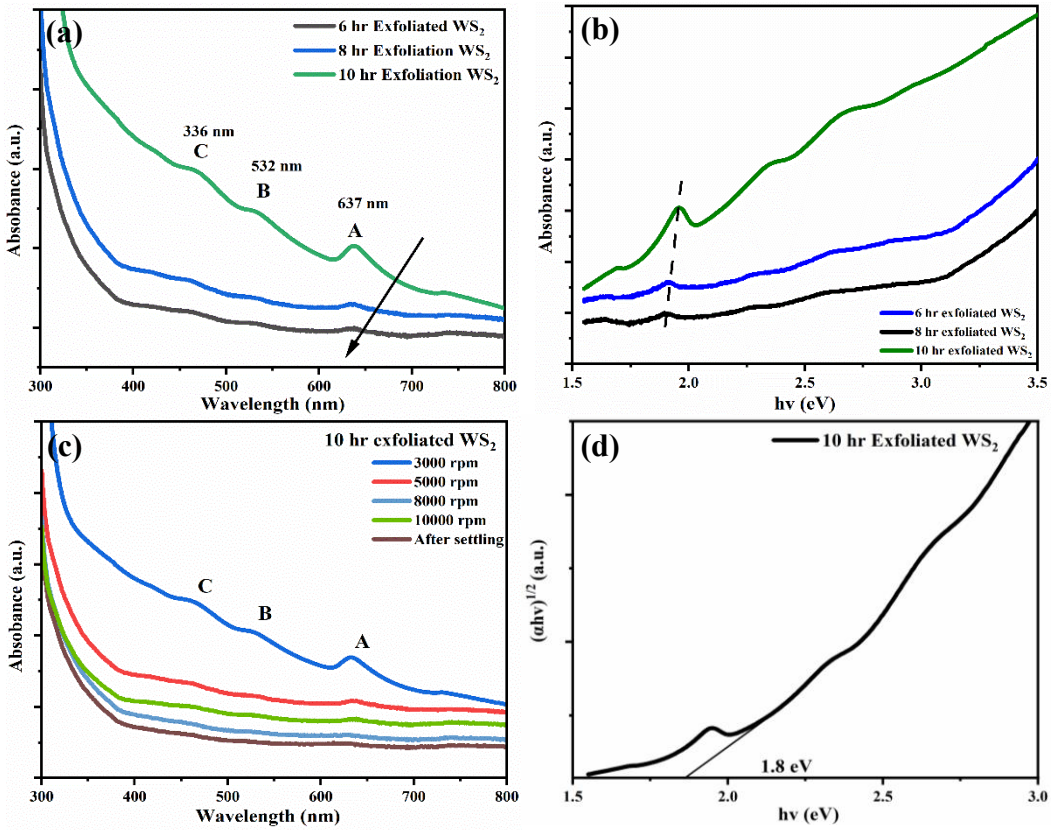

Fig. 3.3: (a) UV-Vis spectra of WS_2 nanosheets at varying exfoliation times (b) correspond UV-Vis plot as a function of energy (hν) (c) after centrifugation at different speeds following 10 hr of exfoliation and (d) Tauc plots of WS_2 nanosheets after 10 hr of exfoliation

3.3.3. Photoluminescence:

The photoluminescence (PL) measurements for the exfoliated WS_2 samples, excited at a wavelength of 532 nm, are shown in Fig. 3.4. PL measurements reveal the bandgap transitions of the WS_2 nanosheets. Emission peaks around ~657 nm, corresponding to the UV-Vis absorbance peak 'A,' were observed for all tested samples. The estimated bandgap corresponding to the ~657 nm emission is approximately 1.89 eV, which aligns well with UV-Vis data [41, 45]. In bulk WS_2, a weak photoluminescence is observed due to its indirect bandgap nature (1.4 eV). However, for the samples exfoliated for 10 hr, narrow emission peaks with higher normalized intensity were observed, indicating reduced thickness and an indirect bandgap semiconductor behaviour [45]. In these exfoliated samples, the indirect bandgap was estimated to be ~1.89 eV, significantly

higher than that of bulk WS_2, with a stronger and more intense peak. In few-layer nanosheets, both spin-orbit coupling and interlayer hopping contribute to valence band splitting at the K points.

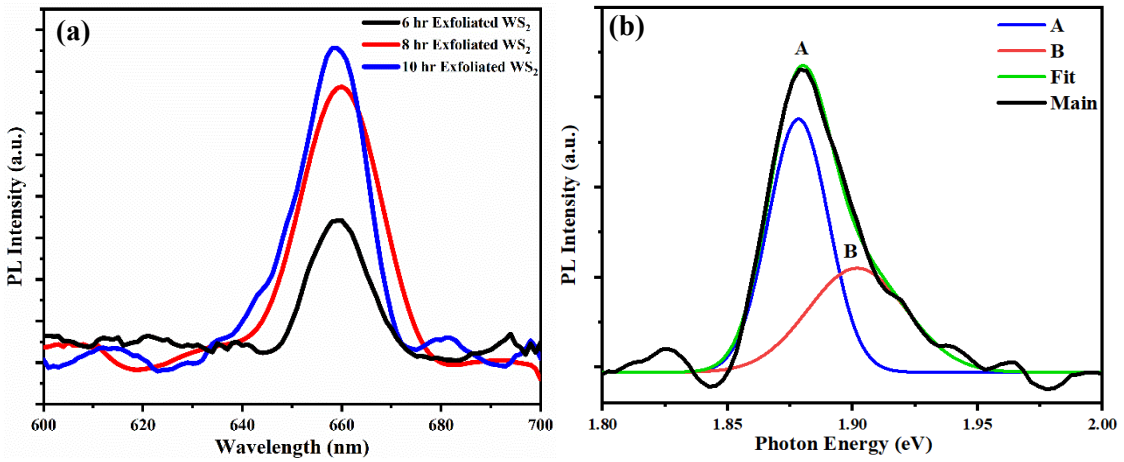

Fig. 3.4: (a) PL Spectra for 6 hr, 8 hr and 10 hr exfoliated WS_2 and (b) Lorentzian functions were used to fit the A and B peaks for 10 hr exfoliated nanosheet

3.3.4. X-Ray Diffraction Spectroscopy:

The XRD patterns of both bulk and exfoliated WS_2 nanosheets, as presented in Fig. 3.5, were analyzed to examine the crystalline structure of the thin-film composed of these nanosheets. For the WS_2 material, a sharp dominant peak observed at 14.5 ^{o} corresponds to 002 plane in 2θ axis indicating the presence of a large number of crystal planes aligned parallel to the *c*-axis [45]. The XRD peak position of the WS_2 nanosheets at the 002 plane indicates the interference pattern of the layered S-Mo-S structure with hexagonal (2H) symmetry [46]. In the XRD spectra for bulk WS_2 multiple weaker diffraction peaks were noticed which correspond to different planes of the existing hexagonal structure of WS_2 and presence of impurity in the bulk WS_2. For the exfoliated sample the diffraction peaks were observed at 2θ plane of 14.5 ^{o}, 29.1 ^{o}, 44.25^o and 60.02 ^{o} which are correlated to (002), (004), (006) and (008) planes of 2H WS_2 nanosheets [47]. The XRD pattern of the WS_2 is matched with the JCPDS card number 08-0237 (P63/mmc space group, 2H-WS_2). A slight decrease in the intensity of the (002) peak for the exfoliated sample was observed and the peaks corresponding to (102), (103), (105) and (110) planes disappeared. This indicates the absence of strong constructive interference from the crystal plane signifying the reduction in layer number [33]. The lattice constant

(c) is 12.1 Å and the interplanar spacing (d) is ~0.6 nm for the XRD peak of 2H-WS_2 at the 002 plane were calculated using Bragg's equation, which aligns well with the HRTEM analysis.

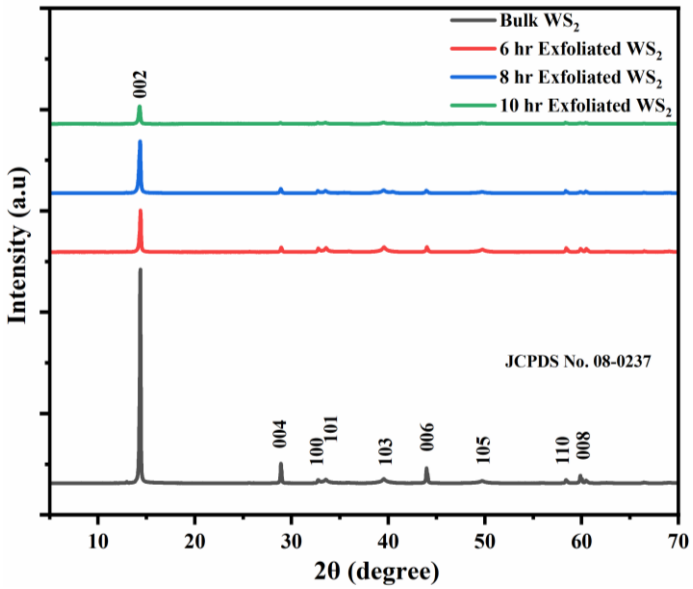

Fig. 3.5: XRD Spectra of the bulk WS_2 powder and exfoliated WS_2 nanosheets at a sonication time of 6 hr, 8 hr and 10 hr

3.3.5. Atomic Force Microscopy:

The representative AFM image and the corresponding height profiles of the exfoliated WS_2 nanosheets as shown in Fig. 3.6. AFM measurements were performed for the thin film of the exfoliated nanosheets on the Si substrate (1x1 cm^2) and measurements were taken with a maximum focusing area of 5 x 5 μm^2. The AFM image of the nanosheets reveals that the shape of the particle is hexagonal symmetry, with sizes spanning a few microns. In bulk form, WS_2 particles have a height exceeding 100 nm, as shown in Fig. 3.6(a-b). Fig. 3.6(c–h) depicts the exfoliated WS_2 nanosheets prepared with varying concentrations of SDBS at 2.29 µmol/ml, 4.30 µmol/ml, and 5.16 µmol/ml. Among these, the sample exfoliated with 5.16 µmol/ml SDBS shows the highest level of exfoliation, achieving flake thicknesses close to 3 nm as shown in Fig. 3.6(g-h). A wider area examination of this extensively exfoliated sample is presented in Fig. 3.6(i), while the related histogram in Fig. 3.6(j) shows the average height distribution of the flakes. The exfoliated nanosheets are noted to possess thicknesses usually under 10 nm, verifying the effective exfoliation of few-layer WS_2 flakes from bulk WS_2. The work reported by

Park et al., Zhang et al. and Li et. al. was demonstrated the estimated thickness of mono and bilayer WS_2 nanosheets to be 0.8-0.9 nm and 1.5-1.6 nm respectively [41,48,49]. Based on these data, it was demonstrated that the exfoliated nanosheets contain ~<10 layers which is consistent with the layer estimation derived using A exciton (λ_A) in UV-Vis spectra. The lateral size of the nanosheets typically ranged from a few nanometers to micrometers. However, after exfoliation, many particles were observed to have broken into smaller pieces, with the edges of the nanosheets losing sharpness, likely due to effect of sonication.

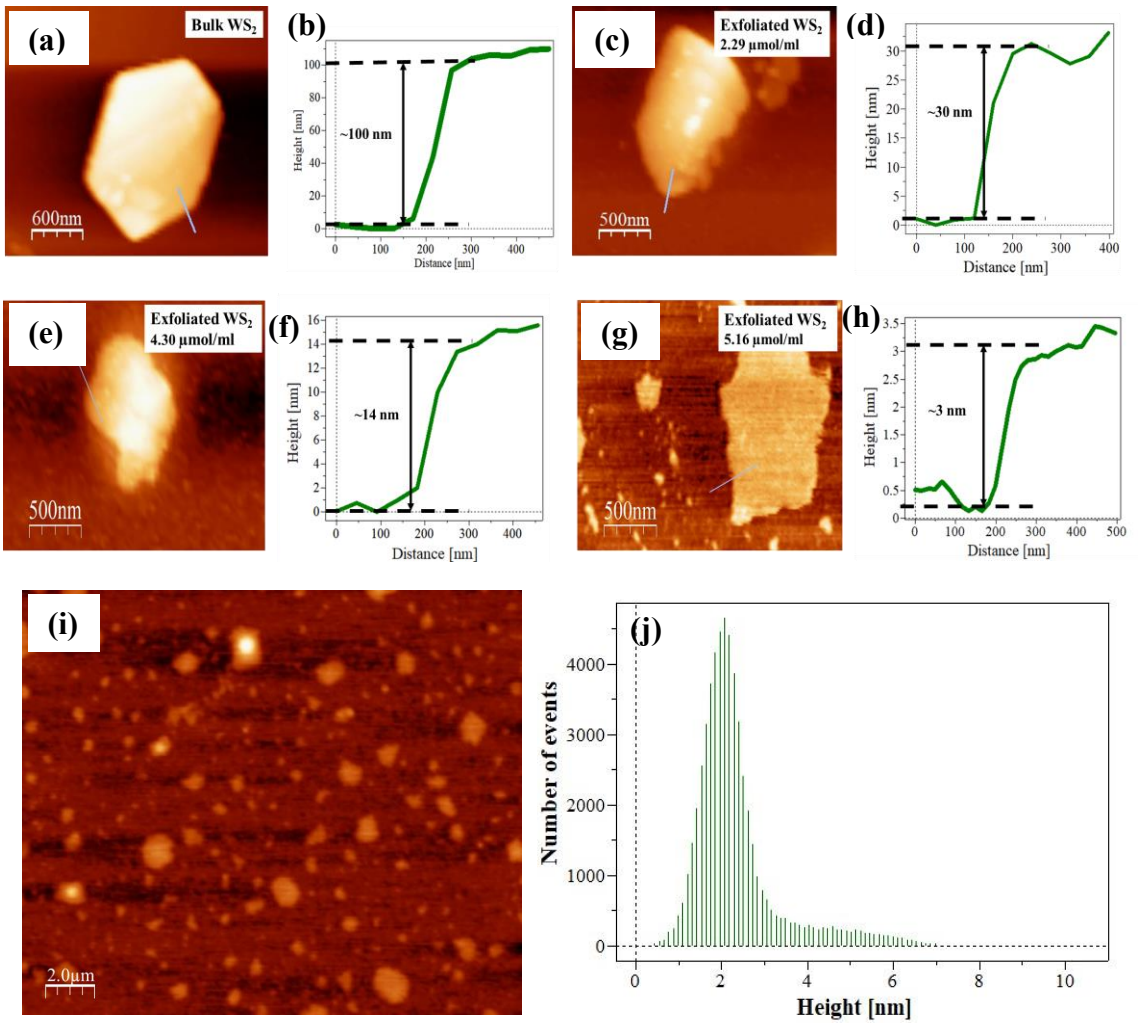

Fig. 3.6: AFM images and corresponding height profiles of WS_2 nanosheets: (a-b) bulk WS_2 flake; exfoliated WS_2 flakes using SDBS at concentrations of (c-d) 2.29 µmol/ml; (e-f) 4.30 µmol/ml; (g-h) 5.16 µmol/ml; and (i-j) wide area AFM image of exfoliated WS_2 flake and corresponding histogram showing the average height distribution

3.3.6. Field Emission Scanning Electron Microscopy:

HRTEM and FESEM analysis is used to study the crystal structure and lateral size of the exfoliated nanosheets. From the representative HRTEM and FESEM images produced in the details of structural symmetry and the nature of exfoliated WS_2 nanosheets were extracted. The FESEM image in Fig. 3.7 (a & b), shows fairly even distribution of hexagonal flakes across the sample surface. The images reveal that the exfoliated WS_2 nanosheets have a lateral size ranging from ~50 nm to ~5 µm and exhibit a hexagonal morphology with a flat, smooth surface and no visible deformations. The hexagonal symmetry indicates that the nanosheets are few-layered, consistent with their 2H-WS_2 semiconducting nature, and the particle shapes closely match the FESEM observations. However, it is observed that prolonged sonication leads to the fragmentation of particles, resulting in their transformation into smaller sizes.

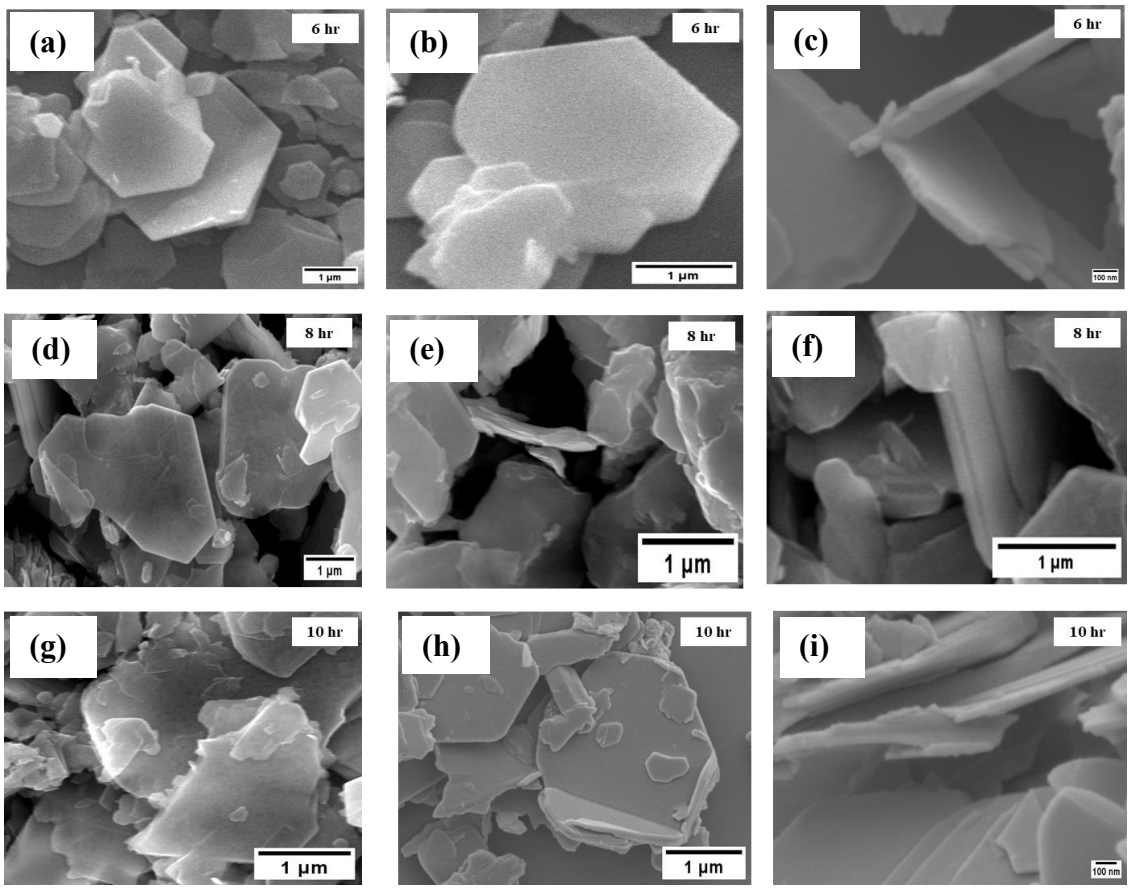

Fig. 3.7: FESEM image of (a-c) 6 hr, (d-f) 8 hr and (g-i) 10 hr exfoliated WS_2 nanosheets

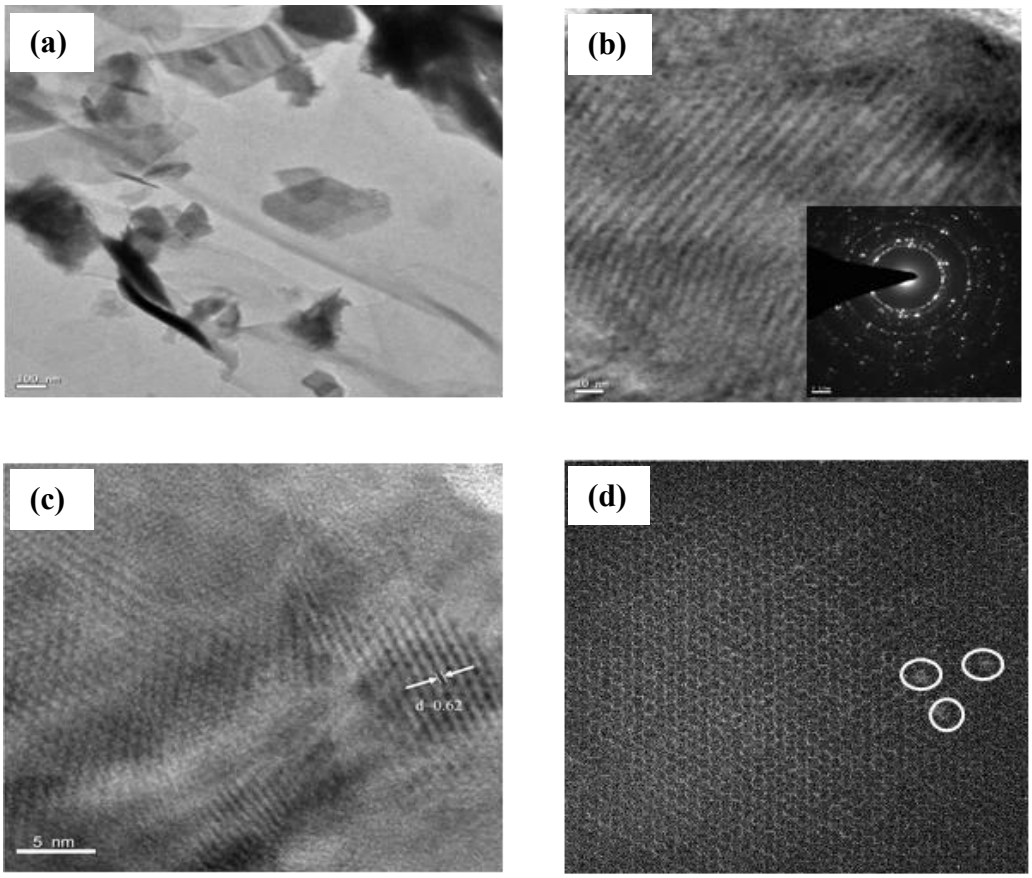

Fig. 3.8: (a) TEM image at lower magnification (b) High-resolution TEM image with corresponding SEAD Pattern at 10 nm scale (c) HRTEM image for exfoliated nanosheets and (d) illustrated the defect in the atomic lattice during the exfoliation

3.3.7. High-Resolution Transmission Electron Microscopy:

Furthermore, the High-resolution transmission electron microscopy (HRTEM) analysis was conducted to ascertain the structural morphology, crystalline properties, and atomic structure of the nanosheets, as depicted in Fig. 3.8. The measurement was carried out initially to determine the particle position on the copper grid, and the image collected is shown in Fig. 3.8(a). The Selected Area Electron Diffraction (SAED) pattern for WS_2 nanosheets was obtained to analyze the crystal structure of the exfoliated nanosheets, as shown in Fig. 3.8(b). At a higher level of magnification, the fringes were noticeable for the nanosheets shown in Fig. 3.8(c) with a lattice spacing of ~0.62 nm taken from the HRTEM image corresponds to the (002) lattice plane that aligns with the (002) peak of the XRD pattern of the exfoliated hexagonal 2H-WS_2 nanosheets depicted in Fig. 3.4.

The results reveal that the nanosheet layers are systematically arranged in line with the orientation of c-axis. The diffraction patterns of the SAED exhibit clear rings that can be linked to the reflections of specific WS_2 planes, such as (002), (006), (110), and (200), showing the hexagonal symmetry of the exfoliated WS_2 flake. The crystal structure of WS_2 is determined to be a hexagonal lattice based on the (002)-diffraction peak in XRD and HRTEM data, aligning with FESEM and AFM findings that show the presence of few-layer nanosheets ranging in lateral dimension from nanometers to micrometers. The results obtained align well with those presented in references [26,49].

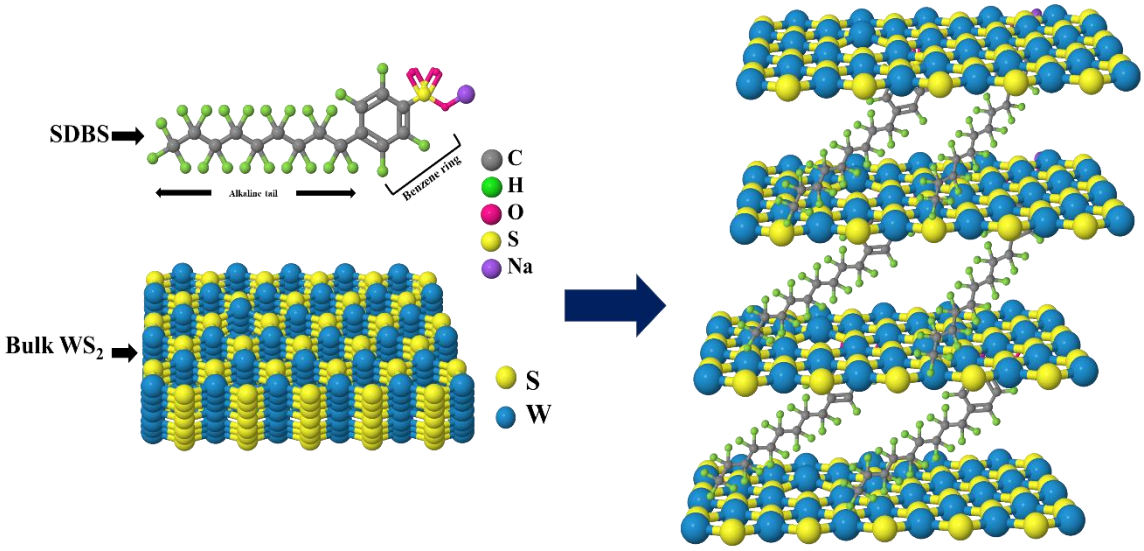

Fig. 3.9: Illustrative representation of the liquid phase exfoliation process of WS_2 nanosheets in an aqueous solvent with SDBS

The exfoliation technique can be explained by the interaction between the non-polar benzene ring and the polar alkyl tail of the amphiphilic surfactant, which preferentially bind to the WS_2 surface in water. This interaction aids in the fragmentation of the bulk material into thin nanosheets. During the exfoliation process, the non-polar head group of SDBS adsorbs onto the nanosheet surfaces, forming a layer of bound charges between them. The resulting electrostatic repulsion weakens the van der Waals forces, preventing aggregation, as shown in Fig. 3.9 [27,49]. Furthermore, the amphiphilic surfactant, with its long alkyl chains, facilitates the formation of micelles in the solution [51,52]. The efficiency of micelles formation is directly related to the concentration of the surfactant in the solution and the exfoliation of nanosheet is

dynamically dependent on the dispersion stability and variation of SDBS concentration. Earlier few researchers reported that the concentration of the surfactant in the exfoliation of graphene and MoS_2 nanosheets was related to the lateral size and thickness of the nanosheets [27]. In this work, the correlation between the concentration of SDBS and the exfoliation efficiency is distinctly observed and is evident from the various spectroscopic measurement data presented here. It is observed that the exfoliation efficiency of WS_2 nanosheets is dependent on the concentration of SDBS. If the concentration of SDBS is increased, the strength of exfoliation of WS_2 also increases. However, beyond a certain limit, which is defined as the critical micelle point of the surfactant (6.02 μmol/ml in the present case), weakening of the exfoliation process is observed. At this critical concentration of the surfactant, maximum exfoliation is achieved resulting in three layers of WS_2 nanosheets.

3.4. Summary:

In this work, we report on a scalable, eco-friendly and straight-forward technique for the synthesis of a few layered WS_2 nanosheets using surfactant assistant liquid phase exfoliation at room temperature. For the identification of the layer number and thickness of the flakes, spectroscopic measurements like Raman spectroscopy, AFM and UV-Vis spectroscopy, PL were used which mutually agreed to the formation of WS_2 nanosheets comprising of few layers. In Raman spectroscopy, the second-order frequency peak 2LA(M) for exfoliated nanosheets is stronger than the bulk WS_2 and the frequency peak difference between E^1_{2g} and A_{1g} is reduced from 69.7 cm^{-1} for bulk WS_2 to 65.15 cm^{-1} for exfoliated WS_2 nanosheet. The calculated layer number of the nanosheet is ~<10 nm was extracted from the A-exciton peak UV- Vis spectra which can determine that the resulting nanosheets are few-layer structures with an indirect bandgap nature of the 2H-WS_2. Additionally, the surface morphology, lateral size and crystalline nature of exfoliated WS_2 nanosheets were examined by AFM, SEM, HRTEM and XRD analysis. The (002) diffraction peak from XRD and HRTEM results coincides with SEM and AFM results revealing the formation of evenly distributed highly crystalline few layers with hexagonal flakes WS_2 nanosheets with a lateral size of few-nanometre to few-micrometer. Also, experimental findings demonstrate that the surfactant concentrations play a critical role in the exfoliation of the nanosheet and a systematic study of the exfoliating efficiency of

SDBS is reported here. The surfactant, SDBS has a critical micelle point of 6.02 μmol/ml, beyond which the process of layer splitting of the WS_2 nanosheet weakens. Highly exfoliated WS_2 nanosheets were obtained at an SDBS concentration of 5.16 μmol/mL. These exfoliated nanosheets were subsequently used for the fabrication of FET devices, and their electrical characterization was thoroughly examined in this thesis.

Bibliography:

[1] Mishra, A. K., Lakshmi, K. V., & Huang, L. Eco-friendly synthesis of metal dichalcogenides nanosheets and their environmental remediation potential driven by visible light. Sci. Rep., 5: 15718, 2015.

[2] Han, G. Q., et. al. WS_2 nanosheets based on liquid exfoliation as effective electrocatalysts for hydrogen evolution reaction. Mater. Chem. Phys., 167: 271–277, 2015.

[3] Kim, D., et al. Thickness-dependent bandgap and electrical properties of GeP nanosheets. J. Mater. Chem. A., 7: 16526–16532, 2019.

[4] Ott, S., Lakmann, M., & Backes, C. Impact of Pretreatment of the Bulk Starting Material on the Efficiency of Liquid Phase Exfoliation of WS_2. Nanomaterials, 11: 1072, 2021.

[5] Yuan, L., et al. A reliable way of mechanical exfoliation of large scale two dimensional materials with high quality. AIP Adv., 6: 125201,2016.

[6] Yan, J., et al. CVD controlled preparation and growth mechanism of 2H-WS_2 nanosheets. Vacuum., 207: 111564, 2023.

[7] Zhang, X., Ma, G., & Wang, J. Hydrothermal synthesis of two-dimensional MoS_2 and its applications. Tungsten, 1: 59–79, 2019.

[8] Coleman, J.N., et al. Two-Dimensional Nanosheets Produced by Liquid Exfoliation of Layered Materials. Science, 331: 568–571, 2011.

[9] O'Neill, A., Khan, U., & Coleman, J.N. Preparation of High Concentration Dispersions of Exfoliated MoS_2 with Increased Flake Size. Chem. Mater., 24: 2414–2421, 2012.

[10] Li, H., et al. Preparation and Applications of Mechanically Exfoliated Single-Layer and Multilayer MoS_2 and WSe_2 Nanosheets. Acc. Chem. Res., 47: 1067–1075, 2014.

[11] Rengifo, S. A Comparison Between Graphene and WS_2 as Solid Lubricant Additives to Aluminum for Automobile Applications, https://digitalcommons.fiu.edu/etd/1862, (2015)

[12] Cong, C., et al. Synthesis and Optical Properties of Large-Area Single-Crystalline 2D Semiconductor WS_2 Monolayer from Chemical Vapor Deposition. Adv. Opt. Mater., 2: 131–136, 2014.

[13] Zhao, Y., et al. Interlayer Breathing and Shear Modes in Few-Trilayer MoS_2 and WSe_2. Nano Lett., 13:1007–1015, 2013.

[14] Behura, S., et al. WS_2/Silicon Heterojunction Solar Cells: A CVD Process for the Fabrication of WS_2 Films on p-Si Substrates for Photovoltaic and Spectral Responses. IEEE Nanotechnol. Mag., 11: 33–38, 2017.

[15] Nagaraju, C., et al. Hydrothermal synthesis of MoS_2 and WS_2 nanoparticles for high-performance supercapacitor applications. New J. Chem., 42: 12357–12360, 2018.

[16] Nicolosi, V., et al. Liquid Exfoliation of Layered Materials. Science. 340: 1226419, 2013.

[17] Backes, C., et al. Guidelines for Exfoliation, Characterization and Processing of Layered Materials Produced by Liquid Exfoliation. Chem. Mater., 29: 243–255, 2017.

[18] Jawaid, A., et al. Mechanism for Liquid Phase Exfoliation of MoS_2. Chem. Mater, 28: 337–348, 2016.

[19] Luo, S., et al. Rational and green synthesis of novel two-dimensional WS_2/MoS_2 heterojunction via direct exfoliation in ethanol-water targeting advanced visible-light-responsive photocatalytic performance. J. Colloid Interface Sci., 513: 389–399, 2018.

[20] Manna, K., et al. Toward Understanding the Efficient Exfoliation of Layered Materials by Water-Assisted Cosolvent Liquid-Phase Exfoliation. Chem. Mater., 28: 7586–7593, 2016.

[21] Cunningham, G., et al. Solvent Exfoliation of Transition Metal Dichalcogenides: Dispersibility of Exfoliated Nanosheets Varies Only Weakly between Compounds. ACS Nano., 6: 3468–3480, 2012.

[22] Halim, U., et al. A rational design of cosolvent exfoliation of layered materials by directly probing liquid–solid interaction. Nat. Commun., 4: 2213, 2013.

[23] Niu, L., Coleman, J.N., Zhang, H., Shin, H., Chhowalla, M., Zheng, Z.: Production of Two-Dimensional Nanomaterials via Liquid-Based Direct Exfoliation. Small, 12: 272–293, 2016.

[24] Sajedi-Moghaddam, A., & Saievar-Iranizad, E. High-yield exfoliation of tungsten disulphide nanosheets by rational mixing of low-boiling-point solvents. Mater. Res. Express, 5: 015045, 2018.

[25] Qin, Y.Q., et al. Ultrathin exfoliated WS_2 nanosheets in low-boiling-point solvents for high-efficiency hydrogen evolution reaction. IOP Conf. Ser. Mater. Sci. Eng., 770: 012079, 2020.

[26] Abhijith, T., et al. Understanding the linear and nonlinear optical responses of few-layer exfoliated MoS_2 and WS_2 nanoflakes: experimental and simulation studies. Nanotechnology, 33: 435702, 2022.

[27] Guan, Z., et al. A facile and clean process for exfoliating MoS_2 nanosheets assisted by a surface active agent in aqueous solution. Nanotechnology, 29: 425702. 2018.

[28] Griffin, A., et al. Effect of Surfactant Choice and Concentration on the Dimensions and Yield of Liquid-Phase-Exfoliated Nanosheets. Chem. Mater., 32: 2852–2862, 2020.

[29] Bogdanova, L.R., et al. Micellization in sodium deoxycholate solutions. Colloid J., 74: 1–6, 2012.

[30] Le, Q.V., et al. UV/ozone-treated WS_2 hole-extraction layer in organic photovoltaic cells. Phys. Status Solidi RRL – Rapid Res. Lett., 8: 390–394, 2014.

[31] Backes, C., et al. Production of Highly Monolayer Enriched Dispersions of Liquid-Exfoliated Nanosheets by Liquid Cascade Centrifugation. ACS Nano, 10:1589–1601, 2016.

[32] Tham, H.M., et al. WS_2 deposition on cross-linked polyacrylonitrile with synergistic transformation to yield organic solvent nanofiltration membranes. J. Membr. Sci., 588: 117219, 2019.

[33] Huang, F., et al. Few-layer thick WS_2 nanosheets produced by intercalation/exfoliation route. J. Mater. Sci., 51: 10160–10165, 2016.

[34] Lotya, M., et al. Measuring the lateral size of liquid-exfoliated nanosheets with dynamic light scattering. Nanotechnology, 24: 265703, 2013.

[35] Meivita, M.P., et al. WS_2 /Polyethylene Glycol Nanostructures for Ultra-Efficient MCF-7 Cancer Cell Ablation and Electrothermal Therapy. ACS Omega, 7: 23075–23082, 2022.

[36] Adilbekova, B., et al. Liquid phase exfoliation of MoS_2 and WS_2 in aqueous ammonia and their application in highly efficient organic solar cells. J. Mater. Chem., C. 8: 5259–5264, 2020.

[37] Ma, L., et al. Scalable exfoliation and friction performance of few-layered WS_2 nanosheets by microwave-assisted liquid-phase sonication. Ceram. Int., 46: 3786–3792, 2020.

[38] Martínez-Merino, P., et al. Novel WS_2 -Based Nanofluids for Concentrating Solar Power: Performance Characterization and Molecular-Level Insights. ACS Appl. Mater. Interfaces, 12: 5793–5804, 2020.

[39] Berkdemir, A., et al. Identification of individual and few layers of WS_2 using Raman Spectroscopy. Sci. Rep., 3: 1755, 2013.

[40] Jeffery, A., et al. Two-Dimensional Nanosheets and Layered Hybrids of MoS_2 and WS_2 through Exfoliation of Ammoniated MS_2 (M = Mo,W). J. Phys. Chem. C., 118: 1386–1396, 2014.

[41] Park, J., et al. Synthesis of uniform single layer WS_2 for tunable photoluminescence. Sci. Rep., 7: 16121, 2017.

[42] Zhou, M., et al. Colloidal preparation and electrocatalytic hydrogen production of MoS_2 and WS_2 nanosheets with controllable lateral sizes and layer numbers. Nanoscale, 8: 15262–15272, 2016.

[43] Baugher, B.W.H., et al. Optoelectronic devices based on electrically tunable p–n diodes in a monolayer dichalcogenide. Nat. Nanotechnol, 9: 262–267, 2014.

[44] Sharma, S., et al. Size-tunable photoluminescence from WS_2 nanostructures. Mater. Res. Express, 5: 045047, 2018.

[45] Choi, Y., et al. Liquid Nitrogen Exfoliation and Nanodispersion of WS_2 for Thermocatalysts. ACS Appl. Mater. Interfaces, 16, 41: 56343–56354, 2024.

[46] Bhatt, P., & Halder, N. Systematic improvement of excitonic features in hydrothermally synthesized WS_2 due to post-synthesis drying. J. Lumin., 266: 120293, 2024.

[47] Qin, Z., et al. Effect of layer number on recovery rate of WS_2 nanosheets for ammonia detection at room temperature. Appl. Surf. Sci., 414: 244–250, 2017.

[48] Zhang, Y., et al. Controlled Growth of High-Quality Monolayer WS_2 Layers on Sapphire and Imaging Its Grain Boundary. ACS Nano, 7: 8963–8971, 2013.

[49] Li, Y., et al. Accurate identification of layer number for few-layer WS_2 and WSe_2 via spectroscopic study. Nanotechnology, 29: 124001, 2018.

[50] Zhang, Y., et al. In situ TEM observation of controlled growth of two-dimensional WS_2 with vertically aligned layers and high-temperature stability. Nano Energy, 67, 104221, 2020.

[51] Vera-López, S., et al. Study of graphene dispersions in sodium dodecylsulfate by steady-state fluorescence of pyrene. J. Colloid Interface Sci., 514: 415–424, 2018.

[52] Gupta, A., et al. Water Dispersible, Positively and Negatively Charged MoS_2 Nanosheets: Surface Chemistry and the Role of Surfactant Binding. J. Phys. Chem. Lett., 6: 739–744, 2015.